Publication II

Ranran Lin and Antero Arkkio. 2009. Calculation and analysis of stator end-winding leakage inductance of an induction machine. IEEE Transactions on Magnetics, volume 45, number 4, pages 2009-2014.

Calculation and Analysis of Stator End-Winding Leakage Inductance of an Induction Machine

Ranran Lin and Antero Arkkio

Department of Electrical Engineering, Faculty of Electronics, Communications and Automation, Helsinki University of Technology, Espoo, Finland

This paper proposes an improved method for calculating the value of and for analyzing the frequency-dependence of the stator end-winding leakage inductance of an induction machine. The method was based on the stored magnetic energy, which was calculated by a 3-D time-harmonic finite element analysis. In this method, there were no rotary parts in the model of the simulated machine. The results of the analysis show that the stator end-winding is capable of influencing the end of the active region of the machine whereas the influence on the central part of the active region is small. In addition, the phenomenon that the stator end-winding leakage inductance, as well as the magnetic energy in the machine, relates to the frequency of the stator current is explored.

Index Terms—**End-winding, finite element analysis, frequency-dependence, leakage inductance.**

I. Introduction

In A rotating electric machine, the current flowing through the end-winding produces the magnetic flux in the end region, which is usually referred to as end-winding leakage. Albeit small in comparison with the main flux, it may give rise to some harmful phenomena, e.g., eddy current in the core end [1] and in the conductive parts of the end region [2], and magnetic forces on the end-winding [3], [4]. In addition, the total leakage reactance is important to know accurately during the calculation of the starting current and starting torque of an induction machine. The end-winding leakage reactance is a large part of the total leakage reactance.

The structure of the end region is more complicated than that of the active region. In the active region, the vector of the magnetic induction rotates in the plane of electrical steel laminations, namely, 2-D rotating flux [5]. However, the distribution of the magnetic field in the end region is always 3-D, so the analysis of the end region is more complex.

In the past several decades, some studies with respect to the calculation of the end-winding leakage inductance were carried out. Mainly, there were two approaches to its calculation. One was based on the flux linkage linking with the end-winding [8]–[10], and the other was the magnetic energy stored in the end region [12]–[15]. Both analytical methods, e.g., Neumann integral [6], [7], and equivalent magnetic circuits [8], and numerical methods, such as the finite element method (FEM), have been used to carry out the above calculation.

A study [9] reported an analytical calculation based on solving the flux linkage. The shape of the coil ends was modelled as a semicircle so the analytical calculation was rough but fast. In [10], moreover, an analytical formula, proposed in [11], was used to calculate the inductance of a current-carrying conductor for switching transient studies.

In another analytical study [6], by applying the method of images, the influence of the iron core was included. A mathematical description of 3-D diamond winding was stated in detail. The computation was based on Neumann integral and was done under different values of the relative permeability of the iron core. It was found that the calculation of the end-winding reactance was the closest to the measurements when the relative permeability of the iron equalled zero. Reference [7], besides, reported the calculation of the end-winding inductance of a switched reluctance machine by using the similar method as in [6].

On the other hand, the finite element analysis (FEA) has been widely used and the majority of the numerical analyses were based on magnetic energy. Reference [12] calculated the end-winding reactance by a 3-D FEA. In particular, an approach for separating the end-winding reactance from the total stator reactance was explained.

References [13], [14] analyzed the end region of an induction machine through both 2-D and 3-D models. In the 2-D FEA, the end-ring inductance was calculated under different boundary conditions. In the 3-D FEA, the leakage inductance with different degrees of coupling between the stator and rotor were calculated based on the magnetic energy. Finally, the results showed that the end-ring inductance was quite important when the rotor was locked. Another study [15] computed the end-winding reactance of some large synchronous machines. In particular, the influence of the radial cooling ducts was taken into account during the computation.

Furthermore, the end-winding inductance of a linear synchronous motor was calculated based on the flux linkage by a 3-D FEA [16]. However, the shape of the end-winding in the linear synchronous motor was different from that in rotating radial-flux electric machines.

A 3-D FEA can give accurate results but it needs a large amount of computation. Therefore, a quasi-3-D FEA was used in the calculation of the end-winding reactance [17], [18]. The quasi-3-D method assumes that the machine is axis-symmetric and that the field variables are sinusoidally distributed along the circumferential direction.

In this paper, an improved method for calculating the stator end-winding leakage inductance is proposed and also the influence of the excitation frequency of the stator current on the leakage inductance is explored. A 1250-kW induction machine acted as the model and a 3-D time-harmonic FEA was carried out by a commercial software package.

Manuscript received September 27, 2008; revised November 21, 2008. Current version published March 18, 2009. Corresponding author: R. Lin (e-mail: ranran.lin@gmail.com).

Color versions of one or more of the figures in this paper are available online at http://ieeexplore.ieee.org.

Digital Object Identifier 10.1109/TMAG.2008.2010317

II. Numerical Simulation

A. Definition of Stator End-Winding Leakage Inductance

Due to the irregular shape of the stator end-winding, some of the end-winding leakage may distribute in the end of the active region. Also, the fringing flux of the air-gap, belonging to the main flux, goes into the end region. Hence, not all the magnetic flux in the end region is the end-winding leakage. Then, to separate the end-winding leakage from the total magnetic flux accurately is of importance to the calculation.

Furthermore, during the calculation of the end-winding leakage inductance of one phase winding, the following three aspects should be taken into account: the effect of a single coil end, the effect among different coil ends in a phase, and the effect among different phases. It is, however, not suitable to speak of the term, mutual inductance, here, because a coil end is not a closed loop [6].

Though there are some papers dealing with the calculation, a unique definition of it has not been formulated for induction machines so far. In particular, the conditions under which the calculation should be carried out are not unique.

In [13] and [14], the stator end-winding leakage inductance was computed in the models with the rotary parts, so its value varies according to the slip. On the other hand, in [12] and [15], the calculation was done in the models without any rotary parts, which means that the coupling between the stator and rotor did not exist. In this paper, the latter case was applied to the calculation so that its characteristic of frequency-dependence could be determined precisely.

B. Method of Analysis

The approach explained in [12] was improved in this study. In the model, all the rotary parts, i.e., the shaft, rotor iron core, etc., were removed, and then the stator winding was fed by three-phase symmetric current. The calculations below are based on arithmetic mean values, i.e. time-averages over one period.

Physically, there is a single kind of magnetic flux in the machine, namely the total flux [19]. When the rotary parts were removed, the total flux would be produced by the stator winding only and it was not suitable to speak of the main flux any more. As a result, all the flux in the model here was considered as the leakage.

According to the source of the leakage, the leakage in the model was divided into two components: the leakage produced by the stator end-winding, i.e., end-winding leakage defined in Section I, and the leakage produced by the active part of the stator winding. In fact, the latter component in the model here included the slot leakage and tooth-top leakage. However, from the angle of magnetic flux, it was difficult to separate the above two components from the total leakage.

As a result, this study dealt with the problem from the angle of magnetic energy. The total magnetic energy in the model was classified locally. According to its source, the magnetic energy was divided into two components: the energy from the stator end-winding, and the energy from the active part of the stator winding. According to its distribution, moreover, the magnetic energy was divided into another two components: the energy in the end region, and the energy in the active region. The above classification is described as

$$\overline{W}_{\mathrm{m,tot}} = \overline{W}^{\mathrm{src}}_{\mathrm{m,act}} + \overline{W}^{\mathrm{src}}_{\mathrm{m,end}} = \overline{W}^{\mathrm{reg}}_{\mathrm{m,act}} + \overline{W}^{\mathrm{reg}}_{\mathrm{m,end}} \quad (1)$$

where $\overline{W}_{\mathrm{m,tot}}$ denotes the arithmetic mean value of the total magnetic energy in the model; $\overline{W}^{\mathrm{src}}_{\mathrm{m,act}}$ and $\overline{W}^{\mathrm{src}}_{\mathrm{m,end}}$ denote the arithmetic mean values of the magnetic energy produced by the active part of the stator winding and by the end-winding, respectively; and $\overline{W}^{\mathrm{reg}}_{\mathrm{m,act}}$ and $\overline{W}^{\mathrm{reg}}_{\mathrm{m,end}}$ denote the arithmetic mean values of the magnetic energy in the active region and in the end region, respectively.

$\overline{W}^{\mathrm{src}}_{\mathrm{m,act}}$ was proportional to the axial length of the stator iron core l_{Fe}, and $\overline{W}^{\mathrm{src}}_{\mathrm{m,end}}$ remained constant, that is, independent of l_{Fe}. The above relations are stated as

$$\begin{cases} \overline{W}^{\mathrm{src}}_{\mathrm{m,act}} \propto l_{\mathrm{Fe}} \\ \overline{W}^{\mathrm{src}}_{\mathrm{m,end}} = \mathrm{constant}. \end{cases} \quad (2)$$

C. 3-D Geometric Model

A 3-phase, 1250-kW squirrel-cage induction machine was modelled in the simulation. Table I lists its related specifications. Owing to the symmetry and periodicity, the axial length of the model was half of the full length and the cross-section perpendicular to the axial direction was a pole pitch sector. The model did not contain rotary parts. For the analysis, the active region was divided into 40 slices and the thickness of each slice was 10 mm in axial direction. The model and one of the slices are shown in Fig. 1(a) and 1(c), respectively.

TABLE I
Main Specifications of Simulated Machine

Rated power (kW)	1250
Rated frequency (Hz)	50
Full length of stator iron core (mm)	800
Outer diameter of stator iron core (mm)	980
Inner diameter of stator iron core (mm)	670
Number of pole pairs	3
Number of stator slots	72
Number of parallel branches	3
Number of turns in series in a stator coil	3
Coil span of a stator coil (stator slot pitches)	10

The materials of the frame and stator winding were isotropic whereas the iron core was anisotropic in both reluctivity and conductivity. Besides, a linear magnetization characteristic was applied to the iron core since the iron core was not deeply saturated when the rotary parts were removed as mentioned above.

Neither the skin effect nor proximity effect was modelled in the stator winding. The eddy current was taken into account in the other conductive parts, e.g. the stator iron core.

D. Simulation by Time-Harmonic FEA

In the time-harmonic FEA, the stator winding was supplied by three-phase current with the value $N\tilde{I}^{\mathrm{str}}_{\mathrm{ph}}/a$, where $\tilde{I}^{\mathrm{str}}_{\mathrm{ph}}$ is the

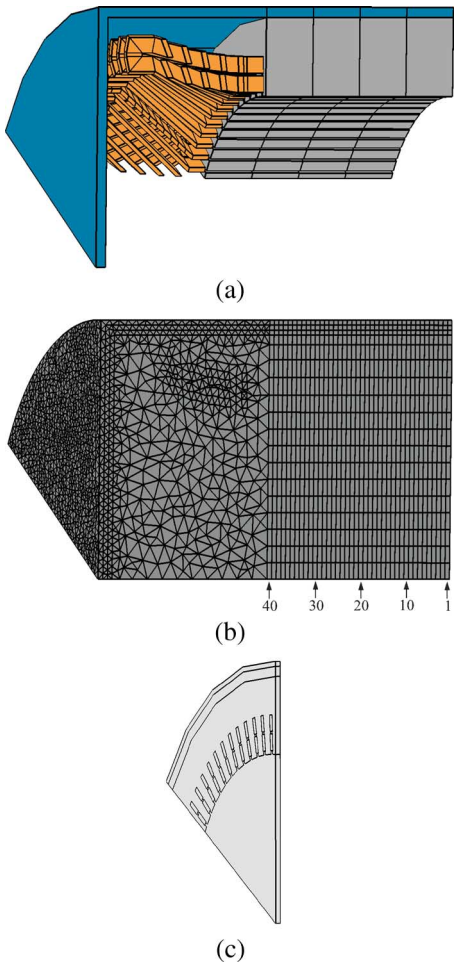

(a) (b) (c)

Fig. 1. The 3-D model of the simulated machine: (a) the geometric model (without the air region); (b) the finite element mesh of the model with the indexes of the slices; and (c) one of the slices of the model for the calculation.

rms value of the stator phase current; N is the number of turns in series in a stator coil; and a is the number of parallel branches. In this machine, $N = 3$ and $a = 3$. The solved governing equation was

$$\nabla \times [\boldsymbol{\nu} \cdot (\nabla \times \underline{\boldsymbol{A}})] + \mathrm{j}\omega\boldsymbol{\sigma} \cdot \underline{\boldsymbol{A}} - \underline{\boldsymbol{J}}_{\mathrm{s}} = \mathbf{0} \tag{3}$$

where ∇ is a vector differential operator; $\underline{\boldsymbol{A}}$ and $\underline{\boldsymbol{J}}_{\mathrm{s}}$ are complex vectors of magnetic vector potential and source current density, respectively; $\boldsymbol{\nu}$ and $\boldsymbol{\sigma}$ are tensors of reluctivity and conductivity, respectively; ω is an angular frequency; and j is the imaginary unit. The eddy-current density $\mathrm{j}\omega\boldsymbol{\sigma} \cdot \underline{\boldsymbol{A}}$ is considered in the conductive parts except in the stator winding. The source current density $\underline{\boldsymbol{J}}_{\mathrm{s}}$ was applied to the stator winding. In the air, there was no current density.

In the $r - \varphi - z$ cylindrical coordinate system, a periodic condition was imposed in such a way that the components of the magnetic vector potential on the two sides of a pole pitch sector, that is, $\underline{A}_r^{\mathrm{I}}$, $\underline{A}_\varphi^{\mathrm{I}}$, and $\underline{A}_z^{\mathrm{I}}$ on one side, and $\underline{A}_r^{\mathrm{II}}$, $\underline{A}_\varphi^{\mathrm{II}}$, and $\underline{A}_z^{\mathrm{II}}$ on the other side, fulfilled the condition: $\underline{A}_r^{\mathrm{I}} = (-1)^k \underline{A}_r^{\mathrm{II}}$, $\underline{A}_\varphi^{\mathrm{I}} = (-1)^k \underline{A}_\varphi^{\mathrm{II}}$, and $\underline{A}_z^{\mathrm{I}} = (-1)^k \underline{A}_z^{\mathrm{II}}$, where k is the number of poles to be simulated. Another condition $\boldsymbol{n} \times \underline{\boldsymbol{A}} = \mathbf{0}$, where $\boldsymbol{n}$ is an outward-directed normal unit vector, was imposed on all the other sides.

Galerkin's method was used in the weak form of the method of weighted residual in order to construct the finite element discretization. Two types of first-order edge-based elements, i.e., tetrahedra and prisms, were used in the end region and active region, respectively. The number of degrees of freedom was 749632. The finite element mesh is shown in Fig. 1(b).

E. Stator End-Winding Leakage Reactance

The proposed method in this paper was based on the magnetic energy. Under a time-harmonic analysis, the arithmetic mean value of magnetic energy density $\overline{w}_{\mathrm{m}}$ is calculated from

$$\overline{w}_{\mathrm{m}} = \frac{1}{T}\int_0^T \frac{1}{2}\mathrm{Re}\{\underline{\boldsymbol{B}}\mathrm{e}^{\mathrm{j}\omega t}\} \cdot \mathrm{Re}\{\underline{\boldsymbol{H}}\mathrm{e}^{\mathrm{j}\omega t}\}\mathrm{d}t \tag{4}$$

where Re means taking the real part of a complex vector; t is time; T is a period; $\underline{\boldsymbol{B}}$ and $\underline{\boldsymbol{H}}$ are complex vectors of magnetic induction and magnetic field strength, respectively. After doing some mathematical operations on (4), the arithmetic mean value of magnetic energy $\overline{W}_{\mathrm{m}}$ in space Ω is

$$\overline{W}_{\mathrm{m}} = \iiint_{\Omega} \frac{1}{4}\mathrm{Re}\{\underline{\boldsymbol{B}}^* \cdot \underline{\boldsymbol{H}}\}\mathrm{d}\Omega \tag{5}$$

where $*$ denotes a conjugate complex vector. The above mathematical operations on (4) can be found in [20].

According to (5), after calculating the arithmetic mean value of the magnetic energy produced by the stator end-winding, $\overline{W}_{\mathrm{m,end}}^{\mathrm{src}}$, the stator end-winding leakage inductance per phase $L_{\boldsymbol{\sigma},\mathrm{end}}^{\mathrm{str}}$ was calculated by

$$L_{\boldsymbol{\sigma},\mathrm{end}}^{\mathrm{str}} = 4p\frac{2\overline{W}_{\mathrm{m,end}}^{\mathrm{src}}}{m\left(\tilde{I}_{\mathrm{ph}}^{\mathrm{str}}\right)^2} \tag{6}$$

where m is the number of phases and p is the number of pole pairs.

III. Results and Analysis

A. Calculation of Magnetic Field

Solving the magnetic field in the model was the first step in the calculation. To ensure the reliability of the solution of the magnetic field, the practical measurements should be the best way. However, it was not possible to make some measurements inside this 1250-kW induction machine. Since the model was not deeply saturated, another method, i.e., the superposition method, was used for comparing the magnetic field in the model, instead.

The time-harmonic FEA was still used in the superposition method. The stator winding was supplied by the current in each phase independently according to its instantaneous complex value. Both the real and imaginary parts of the components of the magnetic induction at some spacial points were computed in the $x - y - z$ Cartesian coordinate system for comparison, and the results are plotted in Fig. 2.

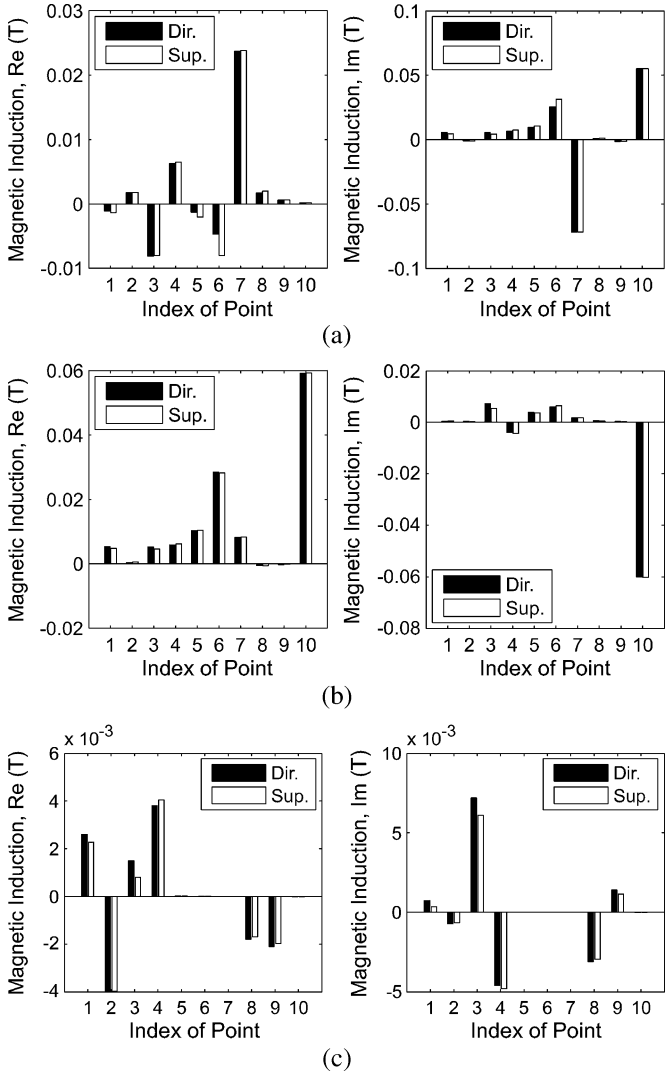

Fig. 2. Real and imaginary parts of the magnetic induction at 10 spacial points by the direct solution and by the superposition method: (a) x-component; (b) y-component; and (c) z-component.

From Fig. 2, the results from the direct solution and from the superposition method are close. That the results are not exactly equal might result from the slightly different meshes used in these two methods. These two methods, to some extent, verified the correctness of the solution of the magnetic field in the numerical model.

B. Stator End-Winding Leakage Inductance

To analyze how the end-winding affects the active region, the arithmetic mean value of magnetic energy, according to (5), was computed in every slice shown in Fig. 1(c). In fact, the magnetic energy in each slice only originated from the leakage in the active region if the influence of the end-winding was omitted. Fig. 3 plots the results in the 40 slices. The indexes of the slices were denoted from 1 to 40 as marked in Fig. 1(b).

In Fig. 3, the arithmetic mean values of the magnetic energy in slices 1–30 are almost equal. Nevertheless, in slices 31–40, that is, the end of the active region, there is an increase along axial direction towards the end-winding. Consequently, the central part

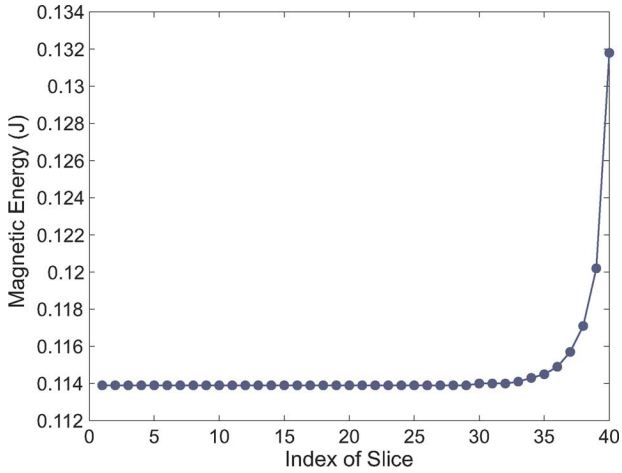

Fig. 3. Arithmetic mean value of the magnetic energy in each slice of the model at the rated frequency.

of the active region (slices 1–30) can be assumed not to be influenced by the end-winding whereas the end part of the active region (slices 31–40) is affected obviously. Hence, a small part of the end-winding leakage enters the end of the active region.

As a result, in this study, slice 1, furthermost from the end-winding, was assumed not to be affected by the end-winding. In other words, $\overline{W}^{\rm reg}_{\rm m,slice1} = \overline{W}^{\rm src}_{\rm m,slice1}$, which means that the arithmetic mean value of the magnetic energy in slice 1, $\overline{W}^{\rm reg}_{\rm m,slice1}$, equalled the magnetic energy from the active part of the stator winding in slice 1, $\overline{W}^{\rm src}_{\rm m,slice1}$. Because 40 slices consisted of the active region, the arithmetic mean value of the magnetic energy corresponding to the total leakage resulting from the active part of the stator winding was

$$\overline{W}^{\rm src}_{\rm m,act} = 40\overline{W}^{\rm src}_{\rm m,slice1}. \tag{7}$$

Therefore, according to (1) and (7), the arithmetic mean value of the magnetic energy related to the end-winding, $\overline{W}^{\rm src}_{\rm m,end}$, was calculated by

$$\overline{W}^{\rm src}_{\rm m,end} = \overline{W}_{\rm m,tot} - 40\overline{W}^{\rm src}_{\rm m,slice1}. \tag{8}$$

At the rated frequency 50 Hz, from (5) and (8), $\overline{W}_{\rm m,tot} = 5.481$ J, $\overline{W}^{\rm src}_{\rm m,slice1} = \overline{W}^{\rm reg}_{\rm m,slice1} = 0.114$ J, and then $\overline{W}^{\rm src}_{\rm m,end} = 0.925$ J. Moreover, $m = 3$, $p = 3$, $\tilde{I}^{\rm str}_{\rm ph} = 270$ A, then from (6), $L^{\rm str}_{\sigma,\rm end} = 101.54$ μH. Then the corresponding stator end-winding leakage reactance per phase is 31.90 mΩ.

Computing the magnetic energy in the end region, $\overline{W}^{\rm reg}_{\rm m,act}$, directly by calculating (5), however, led to a value of 0.894 J. It is smaller than 0.925 J and the relative error is 3.5%. Hence, computing the magnetic energy directly in the end region is not very accurate.

C. Frequency-Dependence of End-Winding Inductance

The stator end-winding leakage inductance of the induction machine was also modelled under different excitation frequencies, i.e., different frequencies of the stator current, in order to find the characteristic of its frequency-dependence.

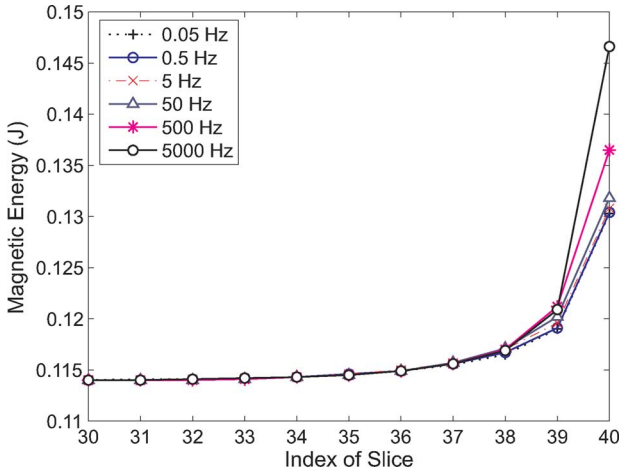

Fig. 4. Arithmetic mean value of the magnetic energy in slices 30–40 of the model under different frequencies.

In this simulation, the only change was the excitation frequency and the other conditions were kept the same. The excitation frequency increased discretely from 0.05 Hz to 5000 Hz with a step of a decade. The arithmetic mean values of the magnetic energy in slices 1–40 under different frequencies were calculated. Because the values of the magnetic energy in slices 1–29 were the same for all the frequencies, only the values in slices 30–40 are plotted in Fig. 4. In Fig. 4, in spite of the excitation frequency, the arithmetic mean values of the magnetic energy in slices 31–40 exhibit an increase towards the end-winding. Also, the higher the excitation frequency is, the more obvious the increase in the magnetic energy becomes. This is due to the influence of the stator end-winding.

The calculations of the frequency-dependence of the stator end-winding leakage inductance and the related magnetic energy are plotted in Fig. 5. As the frequency goes up, the arithmetic mean value of the total magnetic energy in the model decreases but the value of the magnetic energy produced by the active part of the stator winding remains constant. Hence, the value of the magnetic energy produced by the end-winding also decreases, so does the value of the end-winding leakage inductance. When the frequency exceeds 50 Hz, a decrease in their values becomes more distinct.

Besides, Fig. 6 illustrates the comparison between two groups of data corresponding to magnetic energy, i.e., $\overline{W}^{\mathrm{src}}_{\mathrm{m,act}}$ and $\overline{W}^{\mathrm{reg}}_{\mathrm{m,act}}$, and $\overline{W}^{\mathrm{src}}_{\mathrm{m,end}}$ and $\overline{W}^{\mathrm{reg}}_{\mathrm{m,end}}$. Thanks to the influence of the stator end-winding, the magnetic energy in the active region increases as the frequency goes up. On the contrary, the magnetic energy in the end region decreases. The decrease in the end region is more distinct than the increase in the active region, so the total magnetic energy in the model decreases as the excitation frequency rises.

Fig. 6, in fact, proves that $\overline{W}^{\mathrm{src}}_{\mathrm{m,end}} \neq \overline{W}^{\mathrm{reg}}_{\mathrm{m,end}}$ and $\overline{W}^{\mathrm{src}}_{\mathrm{m,act}} \neq \overline{W}^{\mathrm{reg}}_{\mathrm{m,act}}$, in spite of the excitation frequency. The relative errors of these two groups of data are calculated as: $\mathrm{er}^{\mathrm{rel}}_{\mathrm{act}} = |\overline{W}^{\mathrm{reg}}_{\mathrm{m,act}} - \overline{W}^{\mathrm{src}}_{\mathrm{m,act}}|/\overline{W}^{\mathrm{src}}_{\mathrm{m,act}}$, and $\mathrm{er}^{\mathrm{rel}}_{\mathrm{end}} = |\overline{W}^{\mathrm{reg}}_{\mathrm{m,end}} - \overline{W}^{\mathrm{src}}_{\mathrm{m,end}}|/\overline{W}^{\mathrm{src}}_{\mathrm{m,end}}$. Table II lists $\mathrm{er}^{\mathrm{rel}}_{\mathrm{act}}$ and $\mathrm{er}^{\mathrm{rel}}_{\mathrm{end}}$ under different frequencies. Obviously, the relative error in the end region is much more than that in the active region. Moreover, both the relative errors in Table II

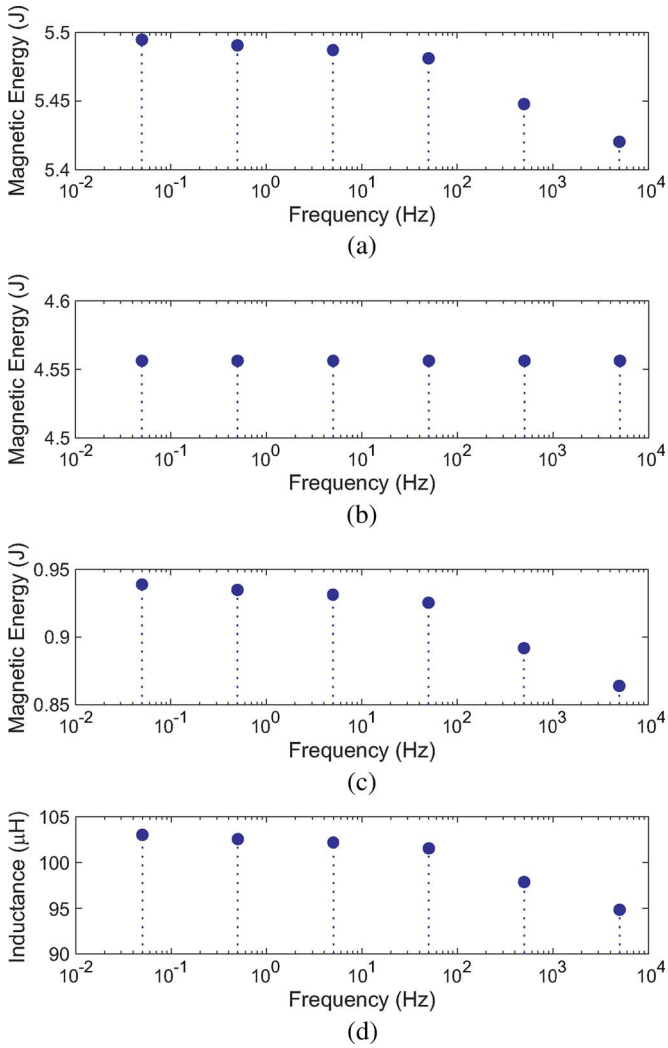

Fig. 5. Analysis of the stator end-winding leakage inductance under different excitation frequencies, 0.05 Hz, 0.5 Hz, 5 Hz, 50 Hz, 500 Hz, and 5000 Hz: (a) $\overline{W}_{\mathrm{m,tot}}$; (b) $\overline{W}^{\mathrm{src}}_{\mathrm{m,act}}$; (c) $\overline{W}^{\mathrm{src}}_{\mathrm{m,end}}$; and (d) $L^{\mathrm{str}}_{\sigma,\mathrm{end}}$.

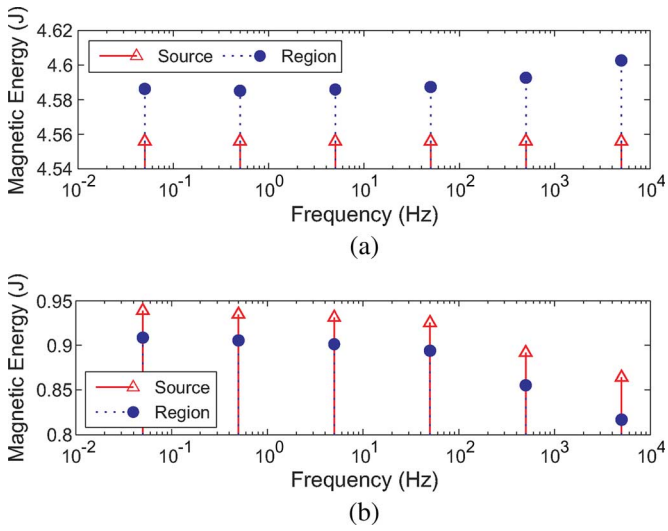

Fig. 6. The comparison of different components of the magnetic energy under different excitation frequencies, 0.05 Hz, 0.5 Hz, 5 Hz, 50 Hz, 500 Hz, and 5000 Hz: (a) $\overline{W}^{\mathrm{src}}_{\mathrm{m,act}}$ and $\overline{W}^{\mathrm{reg}}_{\mathrm{m,act}}$ and (b) $\overline{W}^{\mathrm{src}}_{\mathrm{m,end}}$ and $\overline{W}^{\mathrm{reg}}_{\mathrm{m,end}}$.

TABLE II
RELATIVE ERRORS UNDER DIFFERENT FREQUENCIES

	0.05 Hz	0.5 Hz	5 Hz	50 Hz	500 Hz	5000 Hz
$\mathrm{er}_{\mathrm{act}}^{\mathrm{rel}}$	0.66%	0.64%	0.65%	0.69%	0.80%	1.02%
$\mathrm{er}_{\mathrm{end}}^{\mathrm{rel}}$	3.21%	3.11%	3.21%	3.38%	4.10%	5.48%

do not exhibit an increase at 0.05 Hz, 0.5 Hz, and 5 Hz. This might be caused by the slight numerical errors because these values are quite close.

IV. CONCLUSIONS

In this study, an improved method of calculating the magnetic energy corresponding to the end-winding of a rotating electric machine was proposed in detail. The stator end-winding leakage inductance of a 1250-kW induction machine was computed based on the proposed method. The calculations show that when the rotary parts are removed, the end of the active region of the machine is strongly influenced by the stator end-winding. In addition, the value of the end-winding leakage inductance decreases when the excitation frequency increases. The higher the frequency is, the more distinctly the stator end-winding affects the end region and active region.

This paper, in short, illustrates the calculations of the end-winding leakage inductance and analyzes the influence of the end-winding on the end region and active region under different frequencies. The model of the stator end-winding described here is quite general so the proposed method is also suitable for calculating the end-winding leakage inductance of other radial-flux electric machines.

ACKNOWLEDGMENT

The authors thank M. J. Islam, from the Helsinki University of Technology in Finland, for providing some technical data about the simulated induction machine. This work was supported by the Finnish Foundation for Technology Promotion in Finland, and the Helsinki University of Technology in Finland.

REFERENCES

[1] K. Yamazaki *et al.*, "Eddy current analysis considering lamination for stator core ends of turbine generators," *IEEE Trans. Magn.*, vol. 44, no. 6, pp. 1502–1505, Jun. 2008.

[2] Y. Yao, H. Xia, G. Ni, X. Liang, S. Yang, and P. Ni, "3-D eddy current analysis in the end region of a turbogenerator by using reduced magnetic vector potential," *IEEE Trans. Magn.*, vol. 42, no. 4, pp. 1323–1326, Apr. 2006.

[3] R. Lin and A. Arkkio, "3-D finite element analysis of magnetic forces on stator end-windings of an induction machine," *IEEE Trans. Magn.*, vol. 44, no. 11, pp. 4045–4048, Nov. 2008.

[4] K.-C. Kim, H.-W. Lee, Y.-D. Chun, and J. Lee, "Analysis of electromagnetic force distribution on end winding for motor reliance," *IEEE Trans. Magn.*, vol. 41, no. 10, pp. 4072–4074, Oct. 2005.

[5] Y. Guo, J. Zhu, J. Zhong, H. Lu, and J. Jin, "Measurement and modeling of rotational core losses of soft magnetic materials used in electrical machines: A review," *IEEE Trans. Magn.*, vol. 44, no. 2, pp. 279–291, Feb. 2008.

[6] D. Ban, D. Žarko, and I. Mandić, "Turbogenerator end-winding leakage inductance calculation using a 3-D analytical approach based on the solution of Neumann integrals," *IEEE Trans. Energy Conv.*, vol. 20, no. 1, pp. 98–105, Mar. 2005.

[7] A. Schramm and D. Gerling, "Analytical calculation of the end winding leakage inductance based on the solution of Neumann integrals," in *Proc. IEEE Int. Symp. Industrial Electronics*, Dubrovnik, Croatia, Jun. 2005, vol. 2, pp. 851–855.

[8] K. J. Meessen, P. Thelin, J. Soulard, and E. A. Lomonova, "Inductance calculations of permanent-magnet synchronous machines including flux change and self- and cross-saturations," *IEEE Trans. Magn.*, vol. 44, no. 10, pp. 2324–2331, Oct. 2008.

[9] M.-F. Hsieh, Y.-C. Hsu, D. G. Dorrell, and K.-H. Hu, "Investigation on end winding inductance in motor stator windings," *IEEE Trans. Magn.*, vol. 43, no. 6, pp. 2513–2515, Jun. 2007.

[10] J. L. Guardado and K. J. Cornick, "Calculation of machine winding electrical parameters at high frequencies for switching transient studies," *IEEE Trans. Energy Convers.*, vol. 11, no. 1, pp. 33–40, Mar. 1996.

[11] P. J. Lawrenson, "Forces on turbogenerator end windings," *Proc. Inst. Elect. Eng.*, vol. 112, no. 6, pp. 1144–1158, Jun. 1965.

[12] A. Taieb Brahimi, A. Foggia, and G. Meunier, "End winding reactance computation using a 3D finite element program," *IEEE Trans. Magn.*, vol. 29, no. 2, pp. 1411–1414, Mar. 1993.

[13] R. De Weerdt and R. Belmans, "Squirrel cage induction motor end effects using 2D and 3D finite elements," in *Proc. 7th Int. Conf. Electrical Machines and Drives*, Durham, U.K., Sep. 1995, no. 412, pp. 62–66.

[14] R. De Weerdt, E. Tuinman, K. Hameyer, and R. Belmans, "Finite element analysis of steady state behavior of squirrel cage induction motors compared with measurements," *IEEE Trans. Magn.*, vol. 33, no. 2, pp. 2093–2096, Mar. 1997.

[15] W. M. Arshad, H. Lendenmann, Y. Liu, J.-O. Lamell, and H. Persson, "Finding end winding inductances of MVA machines," in *Proc. 40th Annu. Meeting of the IEEE Industry Applications Society*, Hong Kong, China, Oct. 2005, no. 4, pp. 2309–2314.

[16] A. Tounzi *et al.*, "3-D approaches to determine the end winding inductances of a permanent-magnet linear synchronous motor," *IEEE Trans. Magn.*, vol. 40, no. 2, pp. 758–761, Mar. 2004.

[17] R. Sikora *et al.*, "Analysis of the magnetic field in the end region of induction motor," *IEEE Trans. Magn.*, vol. MAG-18, no. 2, pp. 674–678, Mar. 1982.

[18] Y. Liang and W. Chen, "Numerical calculation of stator end-leakage reactance of large turbogenerator," in *Proc. 5th Int. Conf. Electrical Machines and Systems*, Shenyang, China, Aug. 2001, vol. 1, pp. 170–173.

[19] M. Liwschitz-Garik and C. C. Whipple, *Alternating-Current Machines*, 2nd ed. Princeton, NJ: Van Nostrand, 1961, p. 124.

[20] H. E. Knoepfel, *Magnetic Fields: A Comprehensive Theoretical Treatise for Practical Use*. New York: Wiley, 2000, pp. 240–242.

Ranran Lin was born in Beijing, China, in 1980. He received the B.Sc. degree in engineering from Shanghai Jiao Tong University, Shanghai, China, in 2002, and the M.Sc. degree in technology from the Helsinki University of Technology, Espoo, Finland, in 2004.

He is a Research Scientist with the Department of Electrical Engineering, Faculty of Electronics, Communications and Automation, Helsinki University of Technology. His current research interests include the numerical analysis of electromagnetic field and mechanical vibrations in the end region of large rotating electric machines.

Mr. Lin was a Session Chair of 2008 IEEE International Magnetics Conference held in Madrid, Spain.

Antero Arkkio was born in Vehkalahti, Finland, in 1955. He received the M.Sc. degree in technology and the D.Sc. degree in technology from the Helsinki University of Technology, Espoo, Finland, in 1980 and 1988, respectively.

He has been working on various research projects which deal with the modeling, design, and measurement of electric machines. At present, he is a Professor of electrical engineering at the Helsinki University of Technology. He was a Senior Research Scientist and then a Laboratory Manager at the same university.